

Applications of Finite/Discrete Element Modeling to Rock Engineering Problems

Davide Elmo¹; Doug Stead²; Erik Eberhardt³; and Alex Vyazmensky⁴

Abstract: In this paper, the authors review recent applications of an integrated numerical modeling approach based on the analysis of the mechanical behavior of discrete systems. The numerical analysis includes both a more realistic representation of fracture networks and the simulation of rock mass behavior as a combination of failure through intact rock and displacement/rotation along predefined discontinuities. Selected examples are presented with respect to a variety of engineering problems, including shear testing, failure of hard-rock pillars, slope stability, and block/panel cave mining. The results clearly illustrate the importance of including natural jointing to better capture rock mass behavior in response to loading and unloading. Particular emphasis is given to modeling cave development and surface subsidence, and the proposed numerical method is shown to capture fully the complex rock mass response to caving associated with multi lift extraction. Whereas the use of relatively complex numerical models is progressively becoming widespread in industry, this paper also reviews how numerical simulations of rock mass behavior strongly depends on the geological assumptions used to build the underlying discrete fracture network model and the mechanical properties of the natural discontinuities. Accordingly, a correct balance among engineering judgment, field characterization, and numerical modeling should always be maintained to reduce model uncertainty. DOI: [10.1061/\(ASCE\)GM.1943-5622.0000238](https://doi.org/10.1061/(ASCE)GM.1943-5622.0000238). © 2013 American Society of Civil Engineers.

CE Database subject headings: Numerical models; Rock mechanics; Discrete elements; Cracking; Stress analysis.

Author keywords: Numerical modeling; Numerical analysis; Rock mechanics; Discrete modeling; Fracturing processes; Stress.

Introduction

Two main approaches are used for the numerical modeling of fractured rock masses, based on the concept that the deformation of a rock mass subjected to applied external loads can be considered as being either continuous or discontinuous. The main differences between the continuum and discontinuum analysis techniques lie in the conceptualization and modeling of the fractured rock mass and the subsequent deformation that can take place in it. A continuum model reflects mainly material deformation of the system, while a discontinuum model reflects the movement component of the system. A discrete model is a particular case of discontinuum models, which accommodate an explicit representation of jointing.

Equivalent continuum treatments or alternatively the explicit representation of rock mass jointing through discrete element techniques (Barton et al. 1994; Hajiabdolmajid et al. 2002), provide a convenient framework for the analysis of many complex rock engineering problems. These methods have inherent limitations,

particularly for larger structures and for excavation in potentially complex conditions, such as block caving in very strong rock masses (Pine et al. 2007). The continuum approach may circumvent some of the difficulties associated with the discrete method, in terms of complexity of the model and impracticality of modeling every fracture in a deterministic way. However, an intrinsic limitation of the equivalent continuum approach is that the stress acting on a specific fracture is usually not the same as that deduced from the overall stress, because it depends on the stiffness of the fracture itself and on the stiffness of the fracture's surrounding matrix (Cai and Horii 1993). In addition, the relative displacement of blocks and their interlocking, with associated internal moments produced by block rotations, cannot be adequately accounted for in a continuum model. Kinematic considerations are limited to ubiquitous joint constitutive models to simulate anisotropy. The continuum approach trades material complexity for geometrical simplicity, requiring appropriate homogenization techniques to identify the material parameters associated with specified constitutive equations for the equivalent continuum; the homogenization process is usually very complex and valid only over a certain representative elementary volume (Jing 1998).

Compared with continuum modeling, discrete modeling allows for a better consideration of the role of the discontinuities within the rock mass. In a discrete model, a prefractured rock mass is represented as an assemblage of discrete blocks; rock fractures are modeled numerically as interfaces between these blocks. This means that the rock fracture is considered equivalent to a boundary condition, rather than representing a special element as in the finite continuum-based approach. Complex constitutive relations can be used in a discrete model to define contact forces and displacements at the interface of adjacent stressed blocks, and specific fracturing criterion can also be implemented. The limitations of the discrete element method may arise when dealing with incomplete block formation, although the use of a Voronoi tessellation technique has been demonstrated to provide an alternative solution allowing the

¹Assistant Professor, Institute of Mining Engineering, Univ. of British Columbia, Vancouver, BC, Canada (corresponding author). E-mail: delmo@mining.ubc.ca

²Professor, Dept. of Earth Sciences, Simon Fraser Univ., Burnaby, BC, Canada.

³Professor, Geological Engineering, Univ. of British Columbia, Vancouver, BC, Canada.

⁴Senior Geotech Engineer, Kazakhmys Group, Technical Dept., Samal 2, Microdistrict 69A, Almaty 050059, Kazakhstan.

Note. This manuscript was submitted on October 20, 2011; approved on July 6, 2012; published online on September 16, 2013. Discussion period open until March 1, 2014; separate discussions must be submitted for individual papers. This paper is part of the *International Journal of Geomechanics*, Vol. 13, No. 5, October 1, 2013. ©ASCE, ISSN 1532-3641/2013/5-565-580/\$25.00.

building of discrete models with nonpersistent fractures (Alzo'ubi 2009; Franz 2009). Particle flow codes (Potyondy and Cundall 2004) and lattice spring models (Ostoja-Starzewski 2002; Cundall and Damjanic 2009) represent a specific case of discrete models, in which the rock mass is modeled as an assemblage of particles or mass points bonded together. The values of the bond strengths and stiffnesses are typically determined indirectly through numerical calibration using laboratory test data (e.g., triaxial stress-strain curves).

The physical processes and the modeling techniques chosen eventually influence the extent to which discrete fractures can be incorporated into the models. As discussed by Curran and Ofoegbu (1993), irrespective of the approach chosen to incorporate fractures in a numerical analysis, variability and uncertainties associated with the constitutive relations (stresses versus displacements) defined for the characterization of the fracture surfaces affect the quality of the overall results. The problem of scaling laboratory data to obtain a description of the in situ mechanical behavior of fracture surfaces could also affect the quality of the analysis.

Building on the experience of major research work carried out at Simon Fraser University and the University of British Columbia (Vancouver, British Columbia, Canada), this paper reviews and summarizes recent applications of a finite/discrete element method in response to developing a new approach to model intact rock brittle fracture at varying scales and in varying engineering environments. This includes maximizing the use of field data resulting in a three-dimensional model of the natural fracture system, which can then be incorporated within the continuum-based finite element mesh. By modeling the onset of fracture on a continuum basis, established computational models can be employed that have a significant advantage: the planes or directions of fracture propagation do not have to be defined prior to simulation.

The Hybrid Finite/Discrete Element Method

Hybrid finite/discrete element (FDEM) codes combine aspects of both finite elements and discrete elements, and in specific circumstances, the use of fracture-mechanics principles allows the realistic simulation of brittle fracture-driven processes and a full consideration of the failure kinematics [e.g., Pine et al. (2007), Jiang et al. (2009), Barla et al. (2011), and Mahabadi et al. (2012)]. In general terms, the finite element-based analysis of continua is merged with discrete element-based transient dynamics, contact detection, and contact interaction solutions (Munjiza 2004). The numerical analysis of fracturing processes in rock, in addition to its intrinsic discrete/discontinuous nature, has to consider that such problems are often highly dynamic, with rapidly changing domain configurations, requiring sufficient resolution and allowing for multiphysics phenomena. Additionally, contact behavior also gives rise to a very strong nonlinear system response. For these reasons, such problems are typically simulated employing time-integration schemes of an explicit nature (Owen et al. 2004a). Application of dynamic explicit time-integration schemes to multifracturing solids, particularly to those involving high nonlinearity and complex contact conditions, has increased notably in recent years (Owen et al. 2004b).

There are significant advantages in employing a hybrid FDEM solution strategy to model discrete/discontinuous systems, including:

1. A better description of the physical processes involved, accounting for diverse geometric shapes and effective handling of large numbers of contact entities with specific interaction laws;
2. The implementation of specific fracture criteria and propagation mechanisms allows the simulation of the progressive fracture process within both the finite and discrete elements; and

3. Accounting for the full representation of the anisotropic and inhomogeneous effects of natural jointing.

Among the different hybrid FDEM codes currently available, the code ELFEN (Rockfield 2011) incorporates a coupled, elastoplastic, fracture-mechanics constitutive criterion that allows realistic modeling of the transition from a continuum to a discontinuum, with the development of new fractures and discrete blocks, and a full consideration of the failure kinematics. The following sections specifically address constitutive relationships for the ELFEN code (Rockfield 2011).

The Coupled Mohr-Coulomb with Rankine Cutoff Material Model for Compressive Stress States

Within the ELFEN code (Rockfield 2011), the constitutive behavior used to simulate multifracturing of brittle materials is based on the use of a Rankine rotating crack model coupled with a capped Mohr-Coulomb shear criterion. Fracturing because of dilation is accommodated by introducing an explicit coupling between the inelastic strain accrued by the Mohr-Coulomb yield surface and the anisotropic degradation of the mutually orthogonal tensile yield surfaces of the rotating crack model (Klerck 2000; Klerck et al. 2004). The compressive fracture model represents a phenomenological approach in which micromechanical processes are only considered in terms of the average global response. Local isotropy of strength in compression is justified by assuming uniform material heterogeneity, while accumulation of inelastic strain and associated degradation of the tensile strength is necessarily anisotropic and dependent on the loading direction. The solution procedure has been fully validated for numerous engineering problems, including borehole breakout in both weak (limestone) and strong (granite) rocks where the failure mechanisms are distinctly different (Klerck 2000).

For two-dimensional (2D) plane strain, it is apparent that the Mohr-Coulomb failure criterion is independent of the intermediate principal stress σ_2 , resulting in the fracture plane developing within the plane of analysis. Some authors have justified the omission of the term σ_2 on the basis that it does not generally affect the failure mode and on the assumption that the order of influence is comparable to that of the random variation of material properties exhibited by heterogeneous quasi-brittle materials (Mogi 1967; Yumlu and Ozbay 1995). The Mohr-Coulomb yield surface in tension cannot reasonably represent the physically observed plastic flow directions normal to the mutually orthogonal principal tensile planes. The numerical solution most widely adopted in the literature for the amelioration of the Mohr-Coulomb tensile response is the hydrostatic cutoff. This hydrostatic cutoff plane introduces additional return-mapping possibilities at the intersection with the Mohr-Coulomb yield surface. However, although the inclusion of the hydrostatic tensile cutoff can be considered as an improvement over the standard Mohr-Coulomb yield surface, it is not suitable for application to quasi-brittle fracture because of the arbitrary plastic flow directions (Klerck 2000). The same author argued that only the mutually orthogonal tensile planes of the isotropic Rankine yield surface are able to recover the correct plastic flow directions in tension, thus, as an approximation to the anisotropic softening response of physical quasi-brittle materials, the isotropic nonhardening Rankine tensile cutoff emerges as the only feasible cutoff formulation. The Rankine tensile corner introduces additional yield criteria defined by

$$\sigma_i - \sigma_t = 0 \quad \{i = 1, 2, 3\} \quad (1)$$

where σ_i = each principal stress and σ_t = tensile strength. Although at present no explicit softening law is included for the tensile strength, indirect softening does result from the degradation of cohesion according to the following criteria, ensuring that a compressive normal stress always exists on the shear failure plane:

$$\sigma_t \leq \frac{c(1 - \sin \phi)}{\cos \phi} \quad (2)$$

where c = cohesion and ϕ = friction angle.

Meshing Objectivity and Adaptive Remeshing

As discussed in detail in Klerck (2000) and Owen et al. (2004b), The ELFEN code (Rockfield 2011) incorporates a continuous adaptive remeshing tool, which allows potential difficulties associated with deformation-induced element distortion to be overcome, and fine-scale features to be resolved in the solution. Although the energy dissipation in the crack band model implemented within the ELFEN code (Rockfield 2011) is rendered objective by normalizing the softening curve with the specific fracture energy, G_f , the spatial localization is necessarily arbitrary. Localization occurs in individual elements, resulting in the width of localization and the crack band spacing depending on the discretization, i.e., mesh element size. However, this form of mesh dependence is realized in all local failure models, but does not necessarily render their application spurious. Furthermore, because the mesh orientation can result in directional bias of propagating crack bands based on the fact that strain discontinuities exist at the element boundaries, a nonlocal averaging of the damage measure is adopted in each orthotropic direction: this is done to ensure discretization objectivity by introducing a length scale to govern the width of the localization zone (Owen et al. 2004b). The use of relative finer (high-density) unstructured meshes, generated by methods such as Delauney triangulation, prevents crack band propagation from following arbitrary rows of aligned elements (Klerck 2000).

The failure of heterogeneous quasi-brittle material is associated with the stable growth of an extensive nonlinear process zone responsible for the dissipation of energy and the widespread redistribution of stress. This stable fracture process ultimately results in the formation of macroscopic fractures prior to the maximum load being reached. Accordingly, the computational framework for the realization of the continuum-discrete transition requires a form of topological update of the meshed problem, through the definitions of an efficient remeshing procedure.

As part of the computational scheme of the ELFEN code (Rockfield 2011), when the unloading process within a localization zone is complete, a discrete (and physical) crack is inserted. The discrete crack is introduced when the tensile strength in a principal stress direction reaches zero and is orientated orthogonal to this direction.

The insertion of discrete cracks into the quasi-brittle continuum follows three steps (Owen et al. 2004b):

1. Create a nonlocal failure map (weighted nodal averages);
2. Determine fracture feasibility and the order of discrete crack insertion; and
3. Perform the topological update (remeshing). Alternatively, new cracks could be allowed to grow along existing meshed elements, in which case the mesh size should be kept as small as possible (in relation to the problem scale) to reduce any potential mesh dependency.

Integrated Finite/Discrete Element-Discrete Fracture Network Approach

Rock discontinuities can be characterized in terms of their orientation, intensity, and spatial distribution, in addition to their strength and deformability. With the exception of fully explicit modeling of an individual fracture or simplified fracture sets, the use of a

stochastic discrete fracture network (DFN) approach provides the best option for creating realistic geometric models of fracturing, reflecting the heterogeneous nature of a specific fractured rock mass. The basis of DFN modeling is the characterization of each discontinuity set within a structural domain using statistical distributions to describe variables such as orientation, persistence, and spatial location of the discontinuities. The DFN approach maximizes the use of discontinuity data from mapping of exposed surfaces, boreholes, and/or other sources of spatial information (e.g., digital photogrammetry and the use of LiDAR). The typical process involved in the generation of a DFN model for geomechanics analysis is described in Elmo (2006) and Pine et al. (2006). By coupling a DFN model with a geomechanics analysis, the same authors have demonstrated that it is possible to take full advantage of the use of accessible data, notably the intact rock properties and the orientation, persistence, and intensity of discontinuities, while also explicitly accounting for size and shape (scale) effects, as discussed in the next section.

Synthetic Rock Mass Modeling and Analysis of Scale Effects

The influence of specimen size on the strength of intact rock has long been recognized (Hoek and Brown 1980). For an intact rock sample, it is expected that the reduction in strength will be associated with the number of microdefects included in the sample (Pierce et al. 2009). Similarly, it is suggested that the uncertainty in predicting the behavior of a fractured rock mass is also clearly associated with scale effects (Singh et al. 2002; Hoek 2007). Except for either a very closely fractured or largely massive rock mass, the mechanical response is nonuniform because of the orientation, spacing, and persistence of the discontinuities (Pine and Harrison 2003).

Whereas rock mass classification systems are traditionally used to derive properties for numerical analysis of rock engineering problems [e.g., Hoek et al. (1995, 2002)], establishing representative rock mass properties still represents one of the most important challenges in rock mechanics. In recent years, numerical simulations have been increasingly used to develop synthetic rock mass properties (Pierce et al. 2007; Elmo and Stead 2010; Mas Ivars 2010). The synthetic rock mass approach allows modeling equivalent Mohr-Coulomb or Hoek-Brown strength envelopes, including anisotropic effects, by running simulated laboratory test models of fractured rock masses at scales significantly larger than those feasible in the laboratory. The test results can then be incorporated into a continuum finite element, finite difference, or limit equilibrium analysis. To date, synthetic rock mass modeling has been primarily applied to the simulation of biaxial and triaxial loading. However, it is expected that the resistance to failure under both shear and tensile conditions is considered to be more critical for rock slopes. Building on the work by Elmo et al. (2011), selected examples are reviewed here of synthetic shear and tensile testing at the rock mass scale.

Analysis of Hard Rock Pillars

The strength (loading capacity) of a pillar plays a major role in the design of room-and-pillar mining. As described by Nordlund et al. (1995), failure mechanisms in naturally jointed pillars typically include

1. Failure by lateral kinematic release of preformed blocks as a result of the increasing vertical stress;
2. Failure as a result of the formation of inclined shear fractures transecting the pillar [this mechanism is more likely to affect pillars with a relatively low width-to-height (W/H)]; and

- Failure along a set of transgressive fractures occurring if the angle of inclination of the fractures to the pillar principal axis of loading exceeds their angle of friction.

The mechanical response of a pillar is therefore directly linked to the presence of geological structures and these effects would be more noticeable for slender pillars, whereas wider pillars are more likely to fail through a combination of brittle and shearing processes. For instance, Fig. 1 shows examples of a series of numerical simulations using an integrated FDEM-DFN approach to model different failure mechanisms found in both slender (W/H of 0.5) and wider pillars (W/H of 2).

Similarly, Elmo and Stead (2010) showed that the variation of simulated pillar strength with pillar size for a constant pillar width/height was a function of the pillar width. Furthermore, as the size of the pillar was progressively reduced, it was found that the modeled results agreed qualitatively with the theoretical reduction in rock mass strength for increasing size observed for intact rock specimens (Hoek and Brown 1980). These results demonstrated that it was possible to use a FDEM-DFN fracture mechanics approach as a reliable measure of rock mass strength. Indeed, the mechanical response of a fractured rock mass can be highly variable and, depending on the problem scale, may be too small to account for persistence and termination effects of natural discontinuities in a fully averaged manner. The degree of variability of pillar strength is clearly a function of pillar shape and the numerical analysis has demonstrated that the influence of the jointing intensity progressively reduces for increasing width/height. The scale of the synthetic rock mass tests must be sufficient to capture the representative elementary-volume local jointing conditions and, to account for structural anisotropy, should be repeated to allow for different loading orientations relative

to joint orientations. For instance, anisotropic effects can be induced in a simulated fractured rock mass simply by varying the angle between the applied major principal stress and the direction of the predefined fractures. Preliminary results suggested that anisotropic effects may also be quantified in terms of an equivalent Geological Strength Index (GSI) rating by comparing the modeled strength reduction to the expected Hoek-Brown response for the given rock material (Fig. 2).

Numerical Simulations under Shear Loading Conditions

Karami and Stead (2008) used a FDEM approach to investigate the processes of both joint surface damage and near-surface intact rock tensile failure. Laboratory scales (10 cm) of Selected Barton and Choubey joint roughness coefficient profiles were simulated in direct shear tests and the surface damage mechanisms investigated in terms of tensile fracturing of intact rock along the joint plane. It was shown that the numerical results agree closely with published experimental observations. Additionally, the results show that the joint surface geometry and the applied normal stress directly controlled the dilation along the joint.

Whereas Karami and Stead (2008) considered laboratory scale models, Elmo et al. (2011) focused their study on relatively large simulated rock mass samples, which were sheared under specified normal stresses. The analysis included studying the uncertainties related to different embedded fracture patterns and scale effects by progressively reducing the size of the simulated rock mass sample (Fig. 3). Intact rock and joint material properties used in the models are given in Elmo et al. (2011).

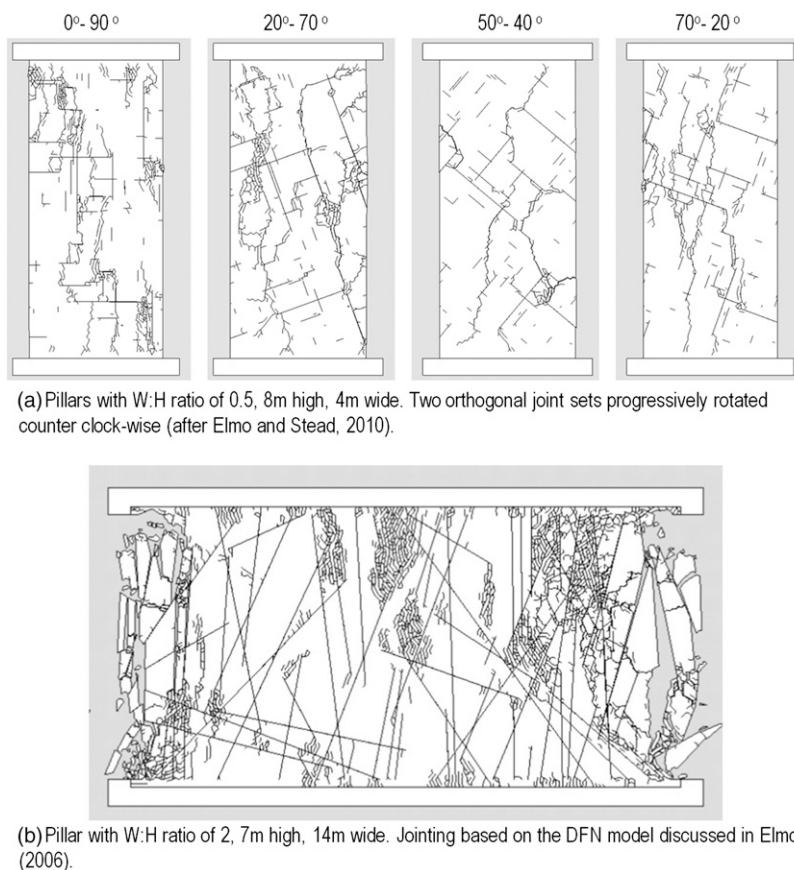


Fig. 1. Modes of failure for selected simulated pillars: (a) W/H of 0.5 and varying fracture orientation; (b) W/H of 2

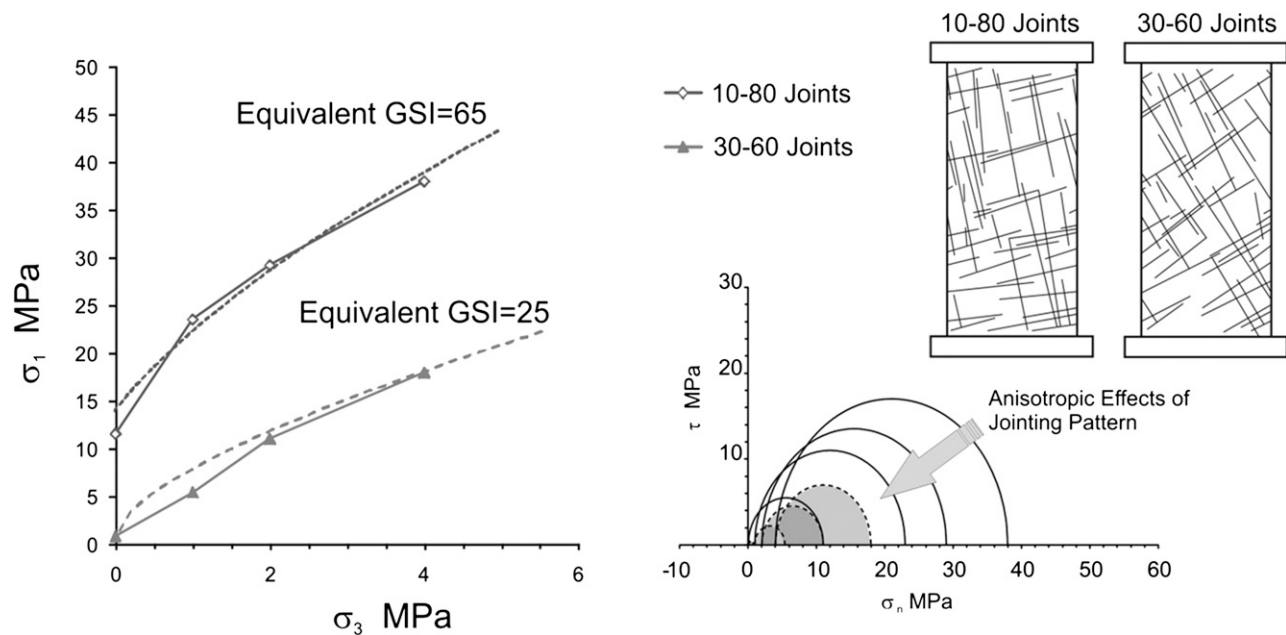


Fig. 2. Simulated anisotropic effects induced in a fractured rock mass by varying the angle between the applied principal stress direction and the inclination of the predefined fractures

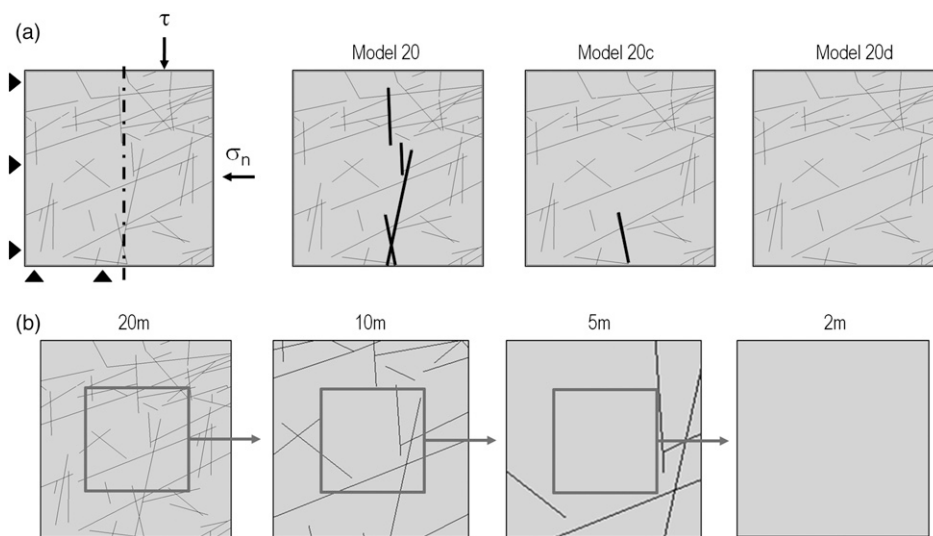


Fig. 3. (a) Loading and boundary conditions for synthetic shear test of a 20×20 m sample; note that in Models Type 20 to 20_d, the fractures aligned close to the direction of induced shearing (shown here in red) have been progressively removed; (b) modeling setup used to analyze scale effects for synthetic rock mass samples under shear loading conditions

Results for the 20×20 -m models are shown in Fig. 4. Depending on the assumed normal stress value, the shear strength of Model 20d is approximately 0.3–0.6 MPa higher than the one simulated for Model 20 [Fig. 4(a)]. It is possible to characterize the strength of the simulated samples at different applied normal stresses as a function of the rock bridge factor, which is herein defined as the ratio between the length of the intact rock portion and the total length of any existing fracture along the vertical axis of the rock sample. The results [Fig. 4(b)] suggest that, for a given applied normal stress, the shear strength of the rock mass sample is directly proportional to the rock bridge factor. It is recognized that the stochastic nature of the DFN process is such that there is an infinite, but equally probable,

number of possible realizations of the 2D fracture systems based on the specified input parameters. Accordingly, to account for uncertainty related to the fracture pattern (i.e., rock bridge potential), it is recommended that several/multiple DFN realizations should be included in any synthetic rock mass modeling program.

As shown in Fig. 5, it is possible to relate the variation of simulated shear strength with increasing sample size to an equivalent GSI value. For assumed isotropic rock mass conditions, the modeled results agree well with the implicit reduction of rock mass strength with decreasing GSI value predicted by the Hoek-Brown criterion. In this context, the results indirectly provide a quantitative interpretation of GSI ratings.

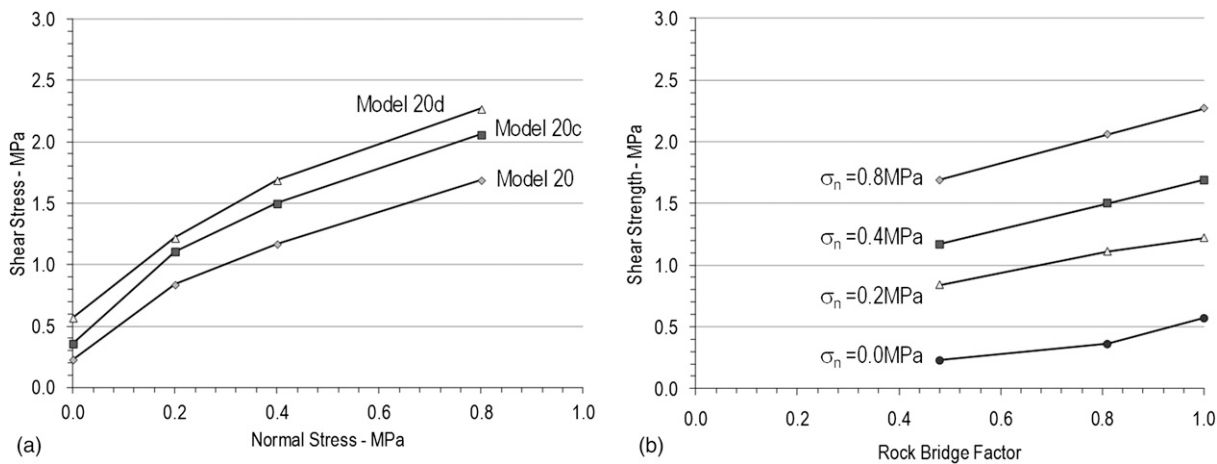


Fig. 4. (a) Results for synthetic shearing tests performed on 20×20 -m models, with the corresponding Hoek-Brown failure response for an intact (small scale) rock sample also given; (b) preliminary characterization of the shear strength of the simulated rock mass as a function of both the applied normal stress and the rock bridge factor along the shearing direction

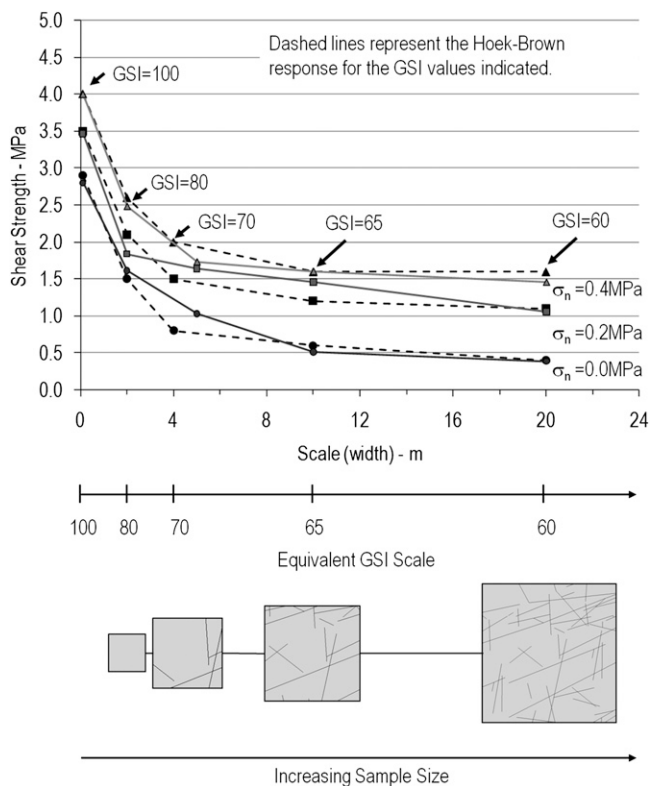


Fig. 5. Preliminary characterization of scale effects to establish a relationship between sample size and rock mass GSI rating

Numerical Simulations under Tensile Loading Conditions

Rock may have significant tensile strength at the intact rock scale; however, at the rock mass scale, discontinuities clearly control the behavior of the rock mass under tensile loading. Although in engineering problems the tensile strength of the rock mass is typically neglected (i.e., taken as approaching zero), it would be reasonable to assume that only under specific (and rare) circumstances could the rock mass be considered as a totally tensionless material. The

measurement of the tensile strength for an intact rock specimen is generally carried out using either indirect (Brazilian) or direct (pulling) tensile tests. In the Brazilian test, a cylindrical specimen is loaded diametrically across the circular cross section, the applied compressive loading causing an extensile deformation (i.e., open splitting) perpendicular to the loading direction. In this study, simulated Brazilian tests have been carried out for fractured rock masses at different scales (20 and 10 m, respectively). Synthetic Brazilian tests included samples with a diameter of 10 and 20 m, respectively [Fig. 6(a)]; varying DFN fracture patterns were included in the current study. Intact rock and joint material properties used in the models are given in Elmo et al. (2011). Fig. 6(b) illustrates the modes of failure for the different rock samples, which, for the indirect Brazilian tests, includes a combination of tensile fracturing of the intact rock material (shown in dark gray) and sliding along the existing discontinuities.

The modeled tensile strength values are shown in Fig. 7. The variation in the underlying DFN fracture pattern explains the modeled range of simulated tensile strength values, characterized by a SD of 0.08 and 0.09 MPa for the rock samples with a diameter of 10 and 20 m, respectively. Considering the absolute magnitude of the measured stresses, the uncertainty indirectly built into the estimation of tensile strength, from the choice of a given fracture pattern, appears therefore to increase with increasing sample size. For instance, for the 10-m-diameter models, the maximum measured tensile stress value is 20% higher than the minimum measured tensile strength, while this difference increases to approximately 60% for the 20-m-diameter models. The results suggest that the rock mass tensile strength is also scale-dependent, as demonstrated for the compressive case, and additionally the results clearly reaffirm the importance of running synthetic rock mass models for multiple DFN realizations.

Brittle Failure Processes for Rock Slopes

The role of brittle fracture in rock slopes has been the subject of considerable research. While the major driving force for this work was originally derived from the need to better understand failure of high mountain slopes, the attention has been gradually shifting to the increasing number of large open pits with projected depths in excess of 1,000 m.

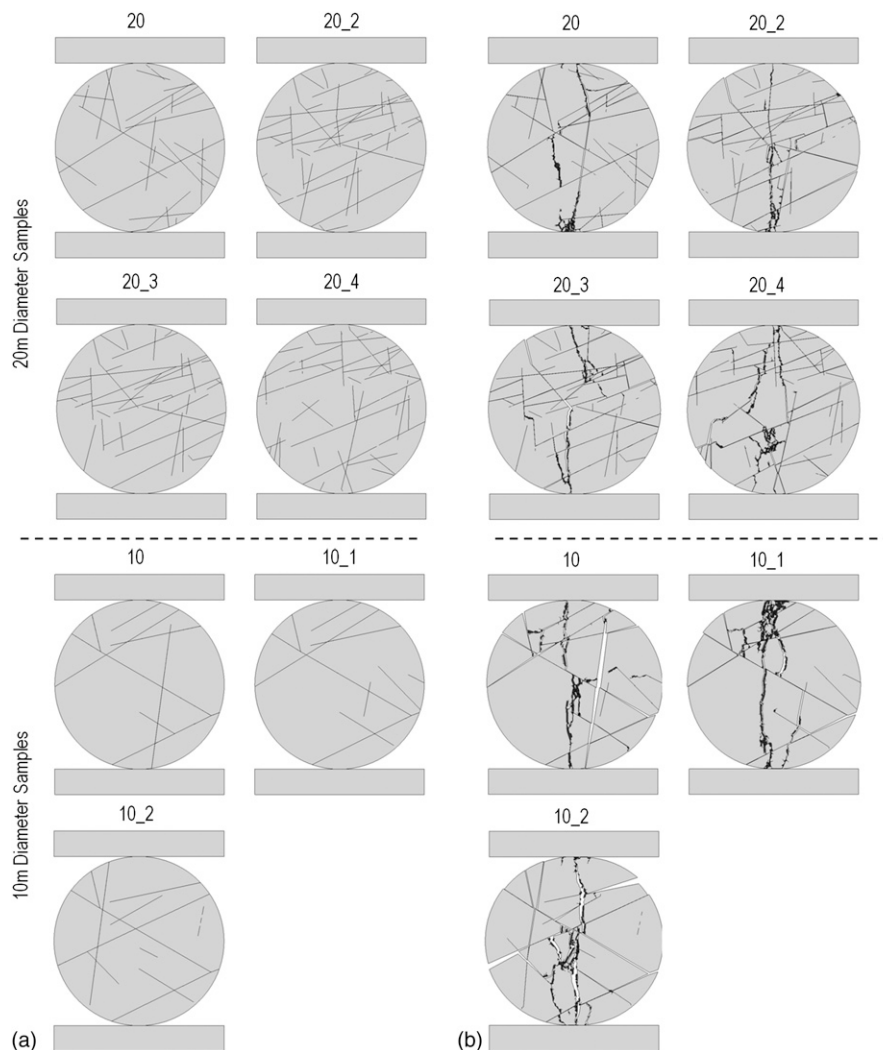


Fig. 6. Synthetic rock mass samples used to simulate indirect (Brazilian) tensile tests, 10- and 20-m diameter and modes of failure for the synthetic rock mass samples simulated under indirect tensile loading conditions; dark gray indicates where tensile failure of the intact rock material has occurred

To date, numerical modeling of rock slopes has generally been undertaken using an elastoplastic Mohr constitutive criterion, and little attention has been given to the validity of plastic deformation in rock slopes and the relationship of the process to the rock slope scale and associated yield stress (Stead et al. 2007). In most situations rock slope failures are controlled by the orientation, shear strength, and stiffness properties of discrete adversely oriented joint planes. The Hoek-Brown criterion and the Geological Strength Index (Hoek et al. 1992, 1995) in their original formulation clearly emphasized that modeling using rock mass properties alone may be inappropriate where discrete structures may potentially control failure. With the exception of weak rock masses, it is safe to assume that in conventional depth open pits (<500 m) or limited height natural slopes, the stresses acting may not be sufficient to cause plastic yield, localization, and failure. Indeed, limited stress concentrations, whether tensile or compressive, are more likely to cause brittle microfracturing. As a result, the overall deformation of the rock slope may be considered plastic, but mechanistically, it develops through extensional brittle fracturing at stresses far below the peak yield strength for the rock mass. The key difference in the slope failure simulated by plastic deformations as opposed to the development of tensile microfractures is that, in the latter, the kinematics of the rock slope mass is dynamic and changes with continued deformation (Stead

et al. 2007). Where simulations involve large open pits or high mountain slopes, the potential for plastic yield becomes more relevant. However, it remains difficult to evaluate the relative roles of extensional brittle fracturing and compressive plastic yield. Realistic simulation requires, therefore, discontinuum models capable of considering both processes. The question of scale also arises as to over what dimensions can tensile failure processes be realistically simulated.

Several studies (Eberhardt et al. 2004; Stead et al. 2006; Yan 2008; Vyazmensky et al. 2010b) have demonstrated the ability of the FDEM approach [using ELFEN (Rockfield 2011)] to simulate formation of step-path failures and intact rock fracture in rock slope environments. In those models, joints were input with varying dimension intact rock bridges and both the properties of the discontinuities and the rock mass varied in a sensitivity approach to reproduce the formation of through-going step-paths and slope failure [Fig. 8(a)]. Examples of the simulation of the 1991 Randa rockslide in Matter, Switzerland (Eberhardt et al. 2004), first with persistent discontinuities and then with more realistic 20–60 m persistent joints at a spacing of 5–20 m (after), are shown in Figs. 8(b and c), respectively.

To emphasize the diversity of roles and scale of brittle fracture within rock slopes, Stead et al. (2007) have characterized brittle

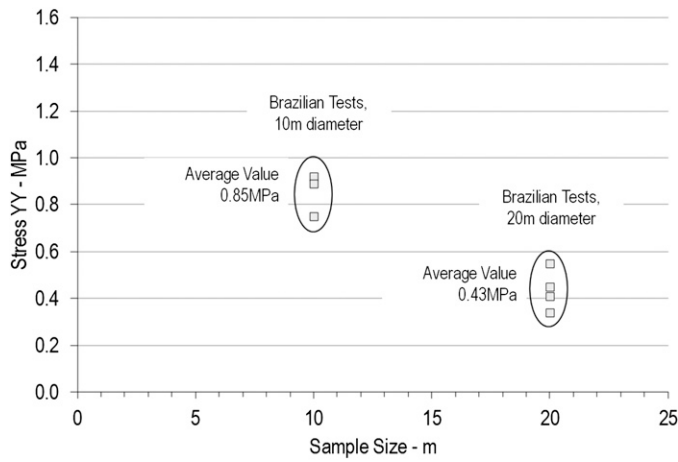


Fig. 7. Modeled tensile strength values for the synthetic Brazilian test models shown in Fig. 6

fracture in rock slopes in terms of primary, secondary, and tertiary processes. These processes are qualitatively described in Fig. 9 through the conceptual simulation of the failure of a rock slope using the FDEM-DFN approach, and are as follows:

- Primary rock slope brittle fracture includes processes that occur prior to the onset of failure, such as: (1) propagation of failure surfaces through fracture tip growth, (2) coalescence of fractures and failure of intact rock bridges, and (3) shearing along discontinuities involving removal of asperities. These processes may lead to rock slope failure through a variety of mechanisms such as sliding along discrete daylighting planes of weakness, step-path failure surface generation, and, in extreme cases, major changes in kinematics through the fracture of keyblocks within a slope.
- Secondary brittle fracture processes may include: (1) development of rear and lateral release surfaces leading toward global slope failure and (2) internal deformation, fracturing, and dilation of the rock slope mass associated with translational failure, toppling, or multiple complex interacting mechanisms. Secondary rock slope brittle fracture processes are associated with a transition from the initiation to transportation stages in a slope failure. They accompany the gradual reduction in rock mass strength and removal of kinematic restraint prior to global rock slope failure and debris transportation.

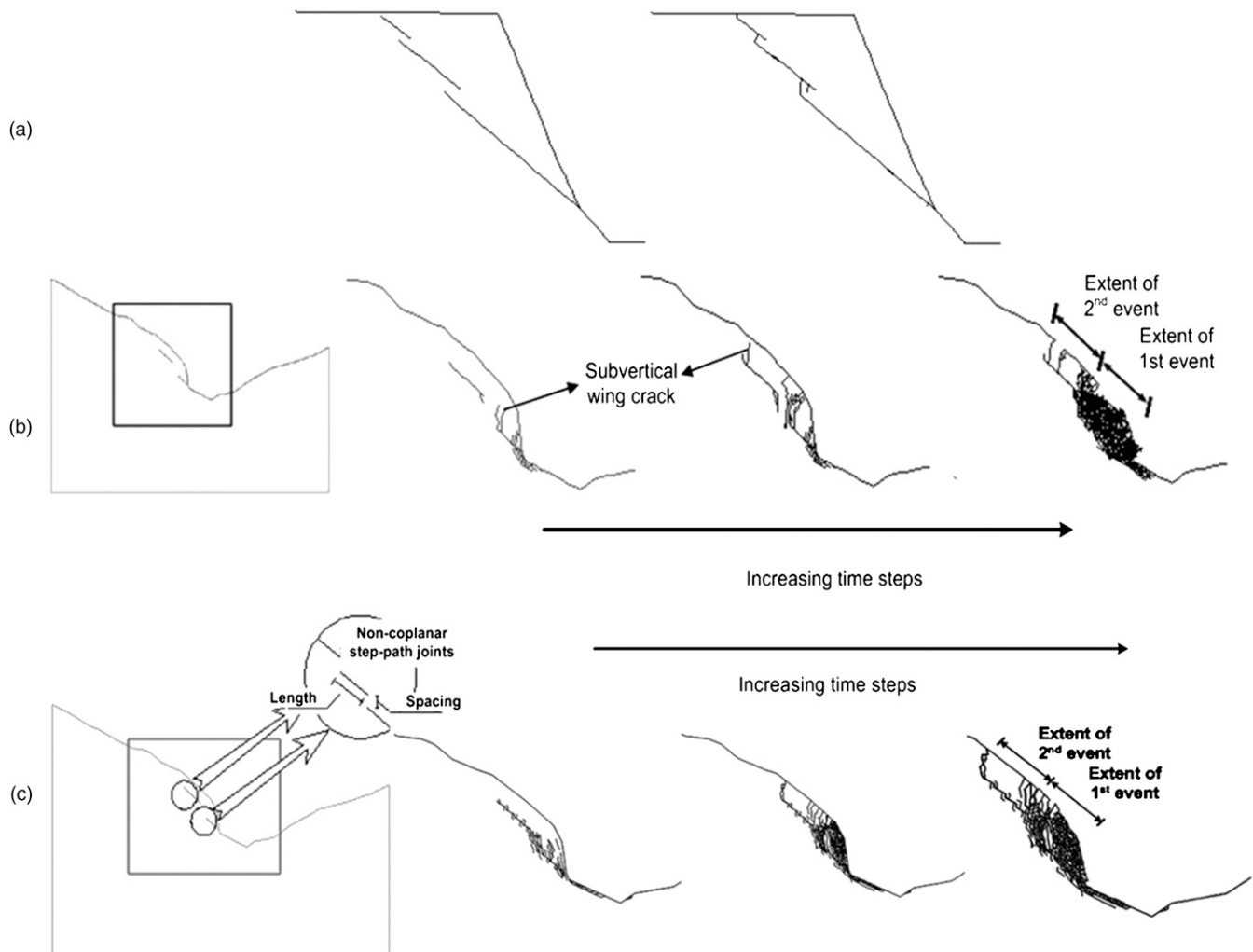


Fig. 8. (a) Initial simplified step-path simulation of a translational failure; simulation of the Randa rockslide assuming: (b) persistent discontinuities and (c) limited persistence discontinuities and step-path failure

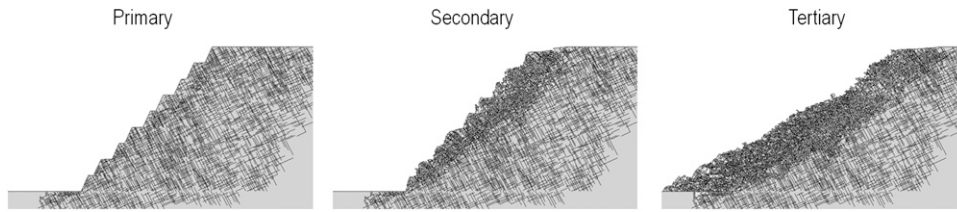


Fig. 9. Qualitative representation and characterization of brittle fracture in rock slopes in terms of primary, secondary, and tertiary processes using a FDEM-DFN approach

- The final stages in the rock slope brittle fracture involves the comminution of the rock mass associated with transport leading up to final debris deposition. These tertiary brittle fracture processes are recognized to be particularly important when characterizing the distance that rock failure debris will travel (run-out) of natural slopes.

Caving Development and Subsidence Analysis

Mass mining (block and panel cave mining) is one of the most cost effective underground mining techniques. High efficiency and low production costs coupled with a growing demand on natural resources have led to the increasing importance of this mining method in the mining industry. A typical cave mine layout consists of two mining levels: an undercut level developed below the ore column to be caved, and a production level beneath the undercut. Ore is mined sequentially in large sections over areas of several thousands of square meters. Caving is initiated by blasting an extensive horizontal panel (undercut) under the ore block to be mined. Stress redistribution and gravity combine to trigger progressive fracturing and caving of the ore into the undercut. As caving of the ore is initiated, the undercut is connected with the production level by blasting ore passages, called drawbells. As the fragmented ore is extracted, the ore above continues to break and cave by gravity. As a result, caving extends progressively upwards, potentially causing significant deformations above the undercut and in the adjacent areas. In this context, the ability to predict surface subsidence associated with block and panel cave mining is becoming increasingly important for mine planning and operational hazard assessment. Owing to problems of scale and lack of access, the fundamental understanding of the complex rock mass response leading to subsidence remains limited, as are current subsidence prediction capabilities. In light of increasing use of the block caving mining method and the importance of knowledge of potential surface subsidence, several studies have been carried out using the proposed FDEM approach to investigate the ability of advanced numerical modeling methods to predict complex rock mass behavior above block cave mines.

Conceptual Studies

Elmo et al. (2007), using relatively simple 2D conceptual caving models with different embedded fracture networks, showed that the location of maximum subsidence was controlled by the orientation of the predefined fracture network. As later discussed by Elmo et al. (2008), a key finding of these initial conceptual models was that the fracture intensity parameter used in the DFN models determined the portion of the natural occurring fractures to be modeled. Because not all natural fractures are represented by the model, the assumed unfractured zones in the model would still contain some degree of fracturing. To account for this, the rock mass properties were scaled accordingly, using a synthetic rock mass approach, as previously discussed.

The work by Vyazmensky (2008) and Vyazmensky et al. (2010a) provided a significant advance in the 2D simulation of fracture and subsidence associated with block caving using a FDEM approach. Valuable insights were gained into the complex mechanisms governing caving-induced rock mass deformations and associated subsidence development. The authors presented numerical models that demonstrated the importance of both joint set orientation and fault location and inclination in determining the mechanisms of subsidence development. Additionally, the governing role of jointing and faulting conditions in defining the degree of surface subsidence asymmetry was demonstrated and a preliminary classification of caving-induced surface subsidence discussed (Fig. 10). One of the major outcomes of the numerical analysis described in Vyazmensky (2008) and Vyazmensky et al. (2010a) was the development of a preliminary classification scheme of block caving-induced surface subsidence (Fig. 11). It is noted that this classification was based on modeling results that assumed a rock mass with a Rock Mass Rating in the range of 50–60, uniform ore extraction, and a block depth of twice the block height.

Finite/Discrete Element-Discrete Fracture Network Modeling of the Proposed Cadia East Panel Cave

The Cadia East Underground Project involves the development of the massive Cadia East deposit into Australia's first panel cave operation. The mine will be the deepest panel cave in the world and Australia's largest underground mine. Mining studies have identified panel caving as the mining method that will deliver the optimum technical and economic outcomes for development of this ore body. It is 100% owned by leading Australian gold producer Newcrest Mining and located within the Cadia Valley Province in central New South Wales, Australia. The Cadia East Underground Project is based on a porphyry zone of gold-copper mineralization adjacent to the eastern edge of the Cadia Hill ore body and extending up to 2.5-km east. The system is up to 600-m wide and extends to 1.9 km below the surface. An integrated FDEM-DFN approach was used at the prefeasibility stage to characterize surface subsidence associated with panel cave mining, focusing on the role of rock mass fabric and faults on surface subsidence development. In particular, the study concentrated on the analysis of two cross sections through the Cadia East ore body, herein named 15100E and 16000E [see (Fig. 12)].

To simulate cave propagation induced by the removal of fragmented ore, a specific algorithm was used that removes all the meshed elements whose centroids are located within a specified region (i.e., corresponding to the undercut/production level in a caving environment). For instance, in the 16000E model under consideration, the undercut width was 300 m, and equivalent boundary forces on the floor and walls of the undercut are then used to simulate the support that the bulked material effectively provides to the surrounding rock mass. An iterative process is used such that the removal of elements is repeated continuously at a given numerical time step to return the specified draw rate, and the model is calibrated to yield a draw rate

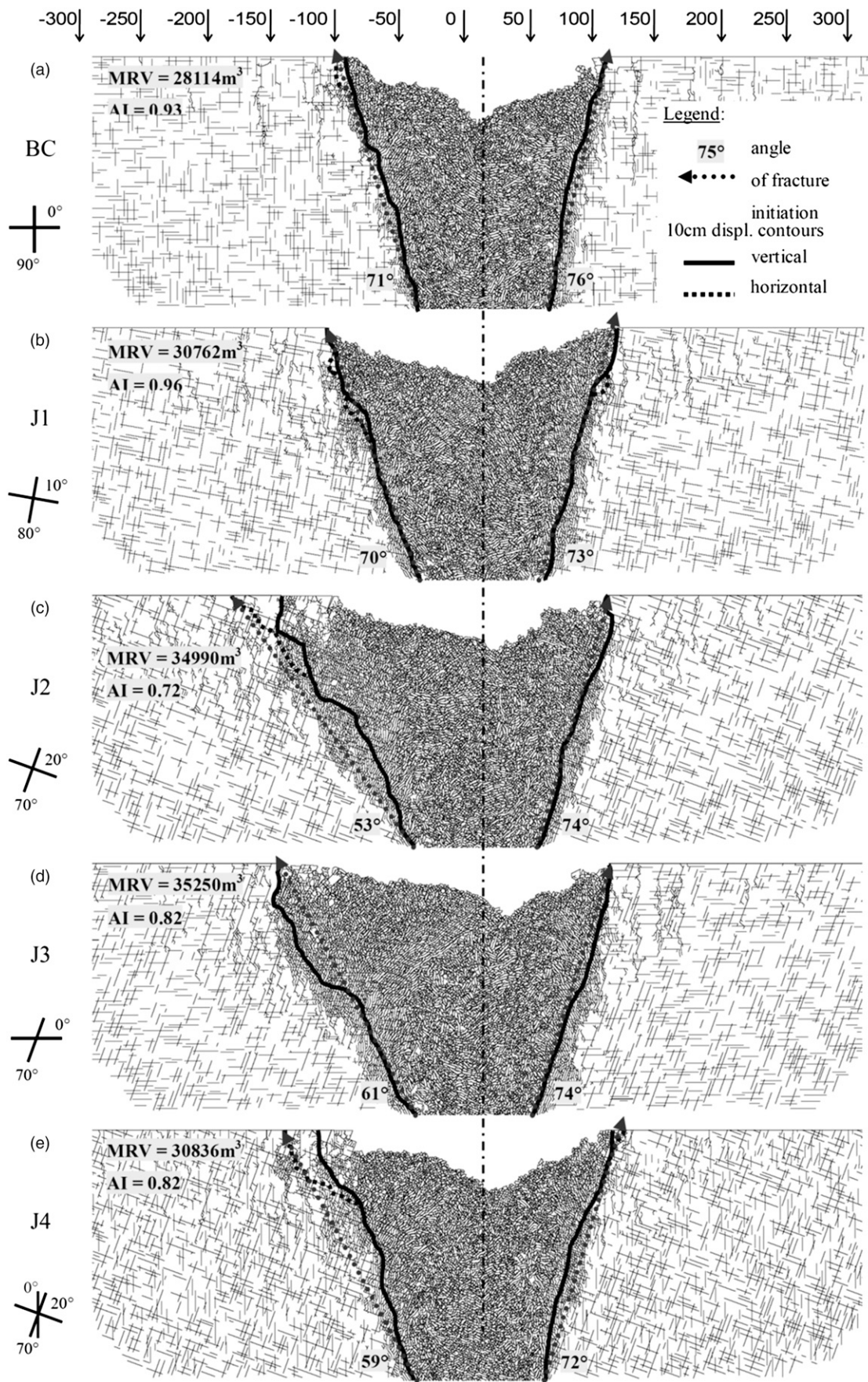
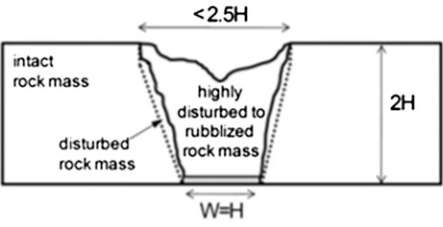
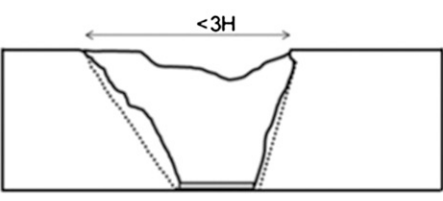
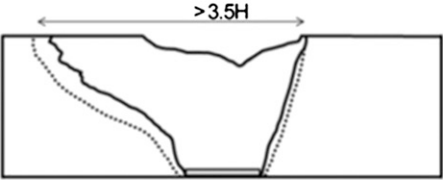


Fig. 10. Selected results of FDEM modeling of cave-induced subsidence, showing subsidence profiles at 100% ore extraction for varying jointing conditions, (a–e) model types [adapted from Vyazmensky (2008), with permission]

Subsidence category	Typical subsidence deformations	Associated rock mass conditions	Min angle of fracture initiation	Asymm. index	Disturbed rock mass volume in % of ore extracted
I. Moderate		Primary controls: combination of vertical/sub-vertical and horizontal/sub-horizontal persistent joint sets, stronger host rock Contributing factors: low horizontal stress	$> 70^\circ$	0.9 - 1	< 220
II. Significant		Primary controls: combination of steeply and low dipping persistent joint sets, Contributing factors: higher joints stiffness	$55^\circ - 70^\circ$	0.7 - 0.9	220 - 250
III. Extensive		Primary controls: combination of steeply and low dipping highly persistent joint sets Contributing factors: high horizontal stress	$< 55^\circ$	< 0.7	> 250

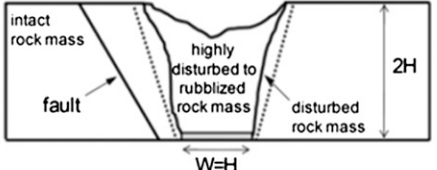
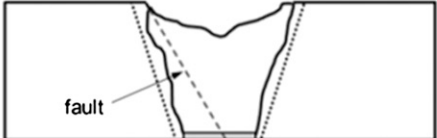
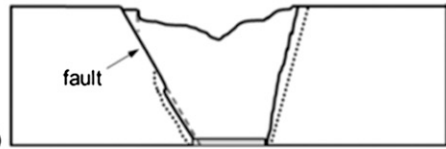
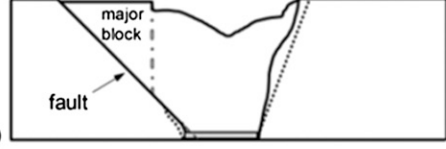
Degree of influence	Typical subsidence deformations	Description
I. Low to Moderate	 I(a)	I(a) fault located at distances exceeding $0.5H$ from the caving boundary <i>fault may act as a displacement barrier limiting rock mass movements in far-field</i>
	 I(b)	I(b) more than $2/3$ of the fault near surface segment is located within caving zone <i>fault may affect caving mechanism</i>
II. Significant to Extensive	 II(a)	II(a) steeply inclined ($80 - 60$) faults intersecting caving boundary
	 II(b)	II(b) moderately inclined ($60 - 30$) faults intersecting caving boundary <i>in both cases extent of surface subsidence and subsidence asymmetry will be governed by fault inclination</i>

Fig. 11. Preliminary classification of the influence of major geological discontinuities on caving-induced surface subsidence based on the results of the FDEM modeling carried out by Vyazmensky (2008) (with permission)

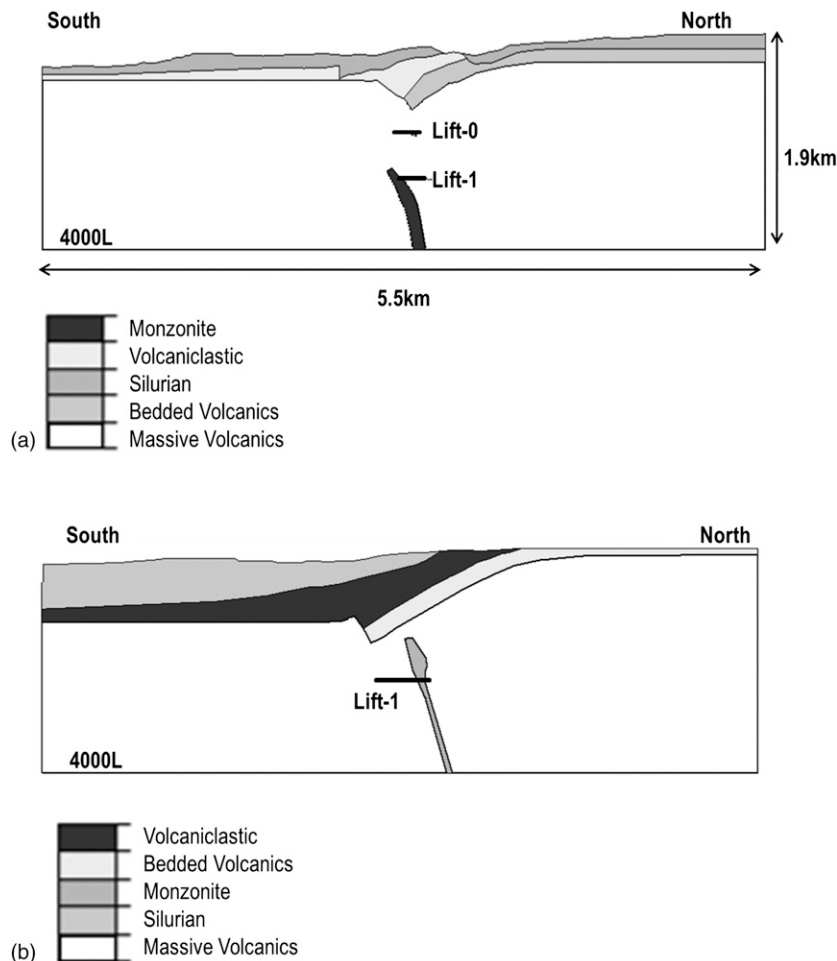


Fig. 12. Cross section through the Cadia East ore body: Model 15100E (a) and Model 16000E (b), respectively

of approximately 100 mm/day. Because of the 2D nature of the modeling, a pseudo-volume of removed ore material had to be defined to constrain the simulated draw rate. The procedure adopted in the current study involved the use of the mine plans provided [specifically, height of draw (HOD), and tons per drawpoint] to define a pseudo-target volume (volume per year), defined as the Mined Block Area (Elmo et al. 2010). Draw zones were defined by grouping together all the drawpoints within ± 15 m of the section azimuth and for each zone an average HOD is calculated. The Mined Block Area was subsequently calculated by multiplying the average HOD by the width of the draw zone, and assuming unit length in the out-of-plane direction, an example for the 16000E model is given in Fig. 13.

Modeling Results: Influence of Rock Fabric and Geological Structures

As shown in Fig. 14, the results for the 16000E model indicate that jointing and major geological faults will have a large impact on cave shape. The presence of the subvertical joint set results in a preferred cave propagation direction, though in the current models the effects of the preexisting joint pattern are minimal compared with the influence of the included geological faults. Up to Year 9.6 the cave appears to be fully contained within two major geological structures. The $[-1\text{ m}, -0.2\text{ m}]$ range of vertical displacement highlights the asymmetric caving-induced deformations, characterized in terms of the angle between the direction of maximum deformation and

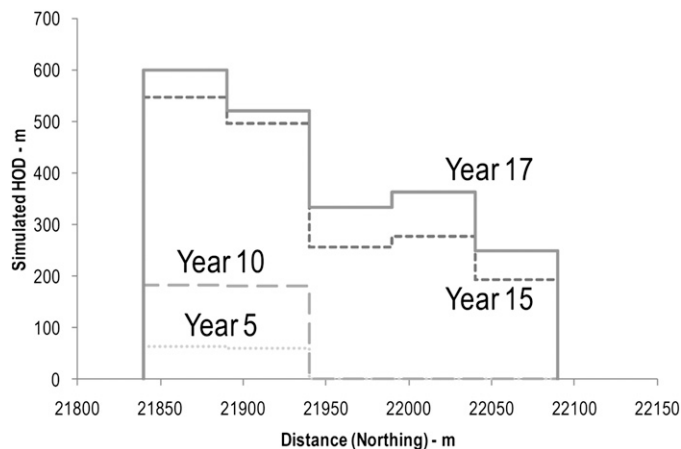


Fig. 13. Mined Block Area at varying stages of the simulation for Model 16000E [adapted from Elmo et al. (2011)]

vertical axis. The crossover occurs when the cave front reaches a point that corresponds to the fault's dip angle varying from steep to shallow. The overall crossover mechanism is clearly influenced by the presence of a north-dipping fault normal to the cave front. Because the caved zone is no longer bounded by the two main faults, its advance becomes predominantly controlled by the subvertical joint set.

In comparison, the 15100E model provided useful indications with respect to cave advance, surface subsidence, and cave interaction between two sequential lifts. The Cadia East Pre-Feasibility Study (Elmo et al. 2010) considered a Lift-0 initiated at Year 1 at the 5150 Level (local coordinate elevation), followed by a Lift-1 at the 4590 Level initiated at Year 15 [see (Fig. 15)]. The occurrence of a subhorizontal joint set is shown in the literature (Vyazmensky 2008) to favor cave propagation, and accordingly the model indicates that the mobilized

cave zone will advance vertically at a relatively rapid rate. In the current model, the failure of the rock bridges between the subvertical set also contributes to control the direction of cave propagation, with the resulting structural features providing low shear strength surfaces for the rock mass to slide under the influence of gravity. In addition, the presence of major geological structures (faults) is shown to influence cave propagation, with the upper Lift-0 cave breakthrough being controlled near the surface by a south-dipping fault.

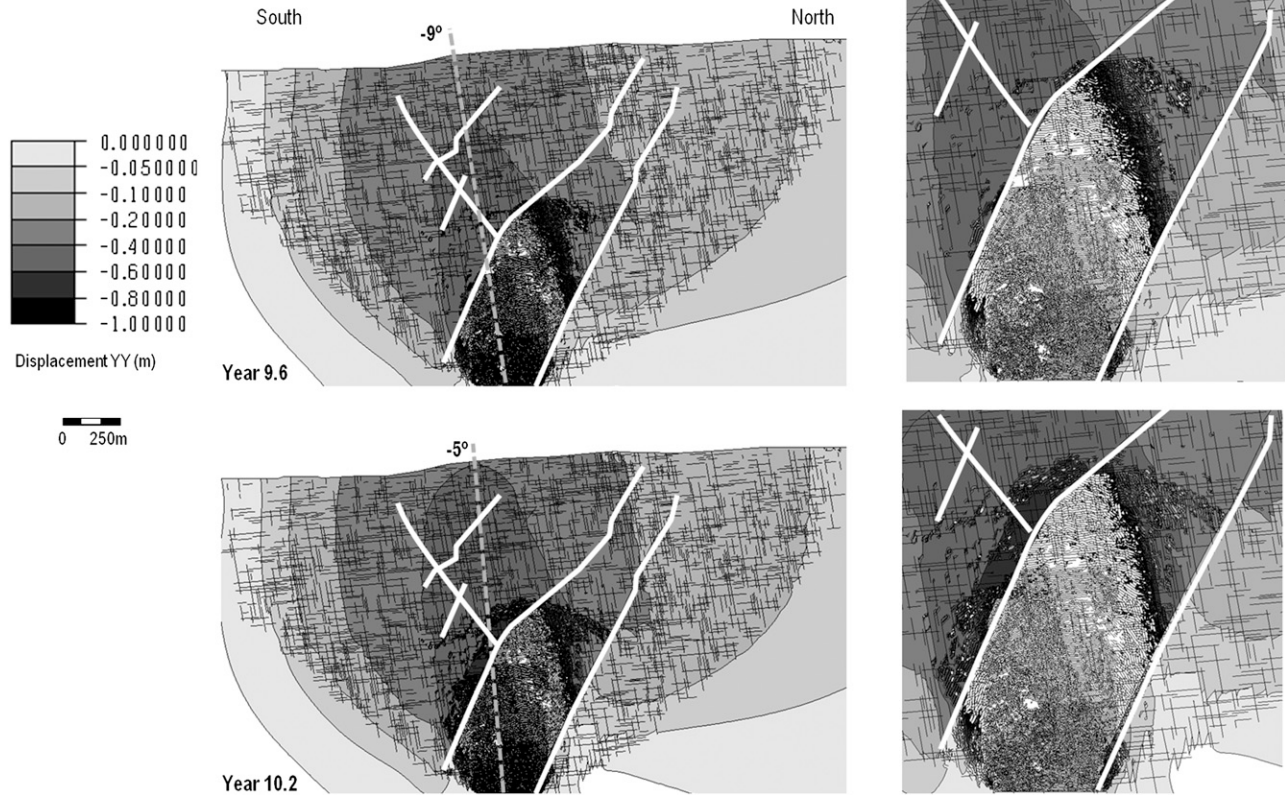


Fig. 14. FDEM results for Model 16000E, showing the simulated impact of major geological faults (lines) and jointing on cave propagation, and the crossover mechanism described in the text

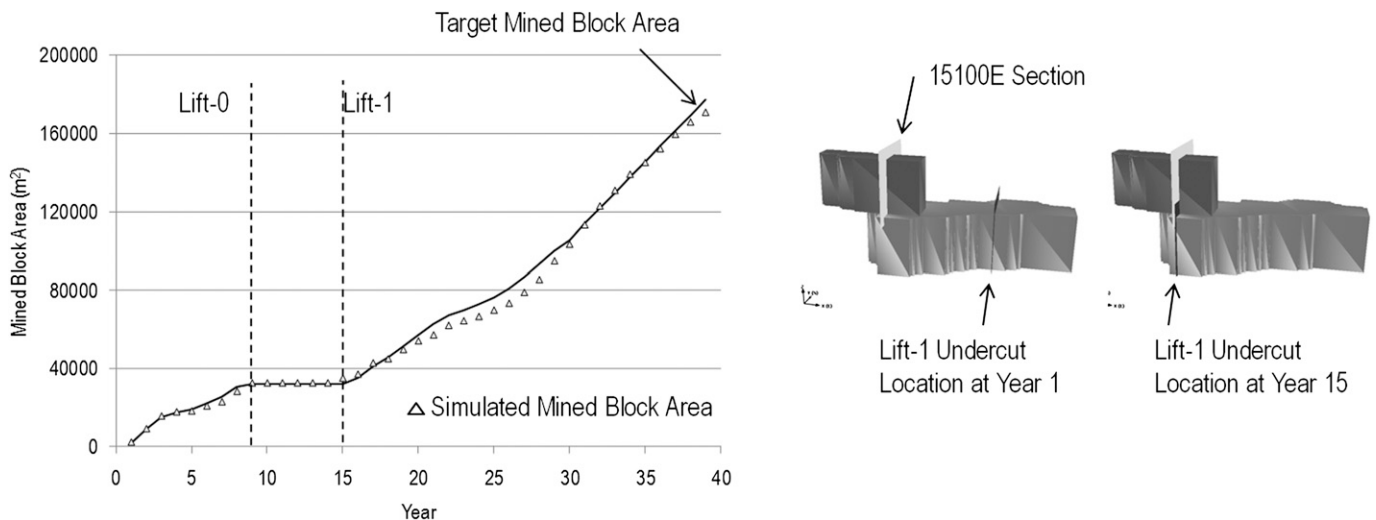


Fig. 15. Comparison between target Mined Block Area for Model 15100E and simulated results (left), with sequence showing the location of Lift-0 compared with Lift-1 as mining progresses

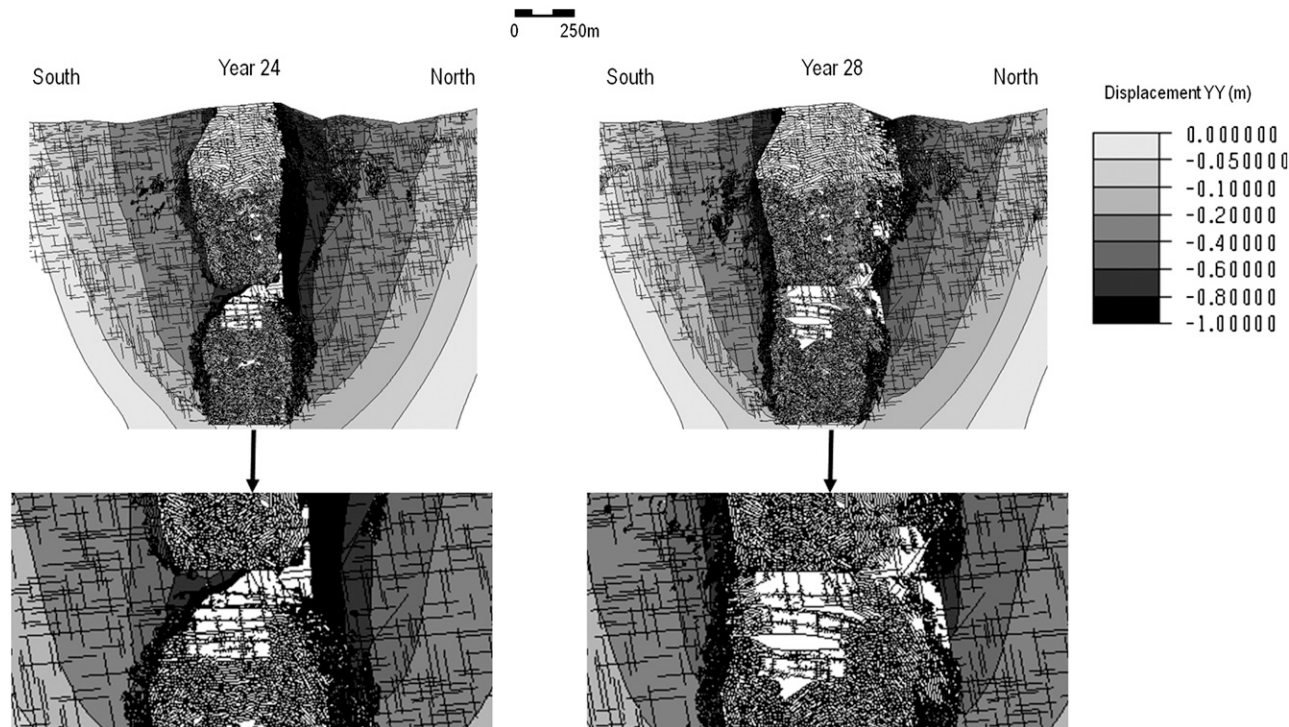


Fig. 16. Model 15100E, simulated interaction between Lift-0 and Lift-1

The interaction between the two caves is controlled by the stress redistribution associated with the presence of the Lift-0 cave, as shown in Fig. 16. The crown pillar between Lift-1 and the overlying Lift-0 initially becomes increasingly stressed, favoring clamping of the subvertical joints and failure through delamination along the subhorizontal joint set. As the caved zone from Lift-1 migrates upwards and connects with the abutments of the Lift-0 extraction level, fractured zones are formed that result in the remnant crown pillar undergoing almost exclusively flexural failure, with large portions of unfractured rock mass becoming mobilized within the distressed cave zone. Because of the lower shear strength of the fractured zones connecting the Lift-1 cave front with the abutments of the Lift-0 extraction level, the simulated failure of the crown pillar is rapid and consequently the caved material left behind in Lift-0 is suddenly mobilized into the underlying Lift-1 cave (Fig. 17). By Year 29 the preexisting faults are almost fully contained within the mobilized caved zone. Accordingly, their influence on cave propagation is no longer apparent. The shape of the cave at Year 29 is almost symmetrical, as indicated by the values of the cave angles.

It is worth noting that the modeling of cave mechanisms for the Cadia East project made no assumptions regarding cave development, which in the model was modeled purely as a function of the assumed rock mass properties, undercut advance, and material extraction. Overall, the results have shown that a discrete fracture modeling approach (FDEM) can effectively capture important cave mechanisms, including preferential rock fragmentation within the ore column and the potential controlling role of rock fabric and geological structures on cave development and surface subsidence.

Conclusions

This paper provides a review and summarizes new applications of an integrated FDEM-DFN using the numerical code ELFEN (Rockfield

2011). In the literature, the approach has been applied to a variety of engineering environments, from laboratory scale to large-scale cave mining and slope problems, under different loading conditions, including compression, shear, and tensile loading. As demonstrated by the cited examples, the proposed numerical approach fully accounts for the anisotropic, inhomogeneous spatial distribution and influence of natural jointing and it is believed the approach can simulate deformation and failure mechanisms in a more realistic way.

With respect to characterization of cave development and surface subsidence, the experience gained to-date using the FDEM-DFN approach has allowed moving from relatively simple and conceptual models, to more sophisticated 2D analyses. Key lessons learned include

1. A numerical analysis is not necessarily simpler only because it is undertaken in a 2D space. The 2D FEM/DEM-DFN modeling approach can effectively capture important cave mechanisms, including preferential rock fragmentation within the ore column and the potential controlling role of rock fabric and geological structures on cave development and surface subsidence.
2. The natural variability of the jointing conditions, including the occurrence of major geological faults, should be modeled whenever possible to account for asymmetric development of the cave front and subsidence crater.
3. For 2D discrete models with fracturing simulation, further studies are required to investigate the impact that the range of stochastically generated DFN realizations may have on the maximum extent of surface subsidence.
4. Improved drawing algorithms were implemented in the analysis to realistically simulate the removal of caved material from the ore column.

This paper reviews recent advances of the FDEM approach for rock engineering applications gained within the last decade. The examples provided show that hybrid finite-discrete element numerical methods have the potential to overcome some of the

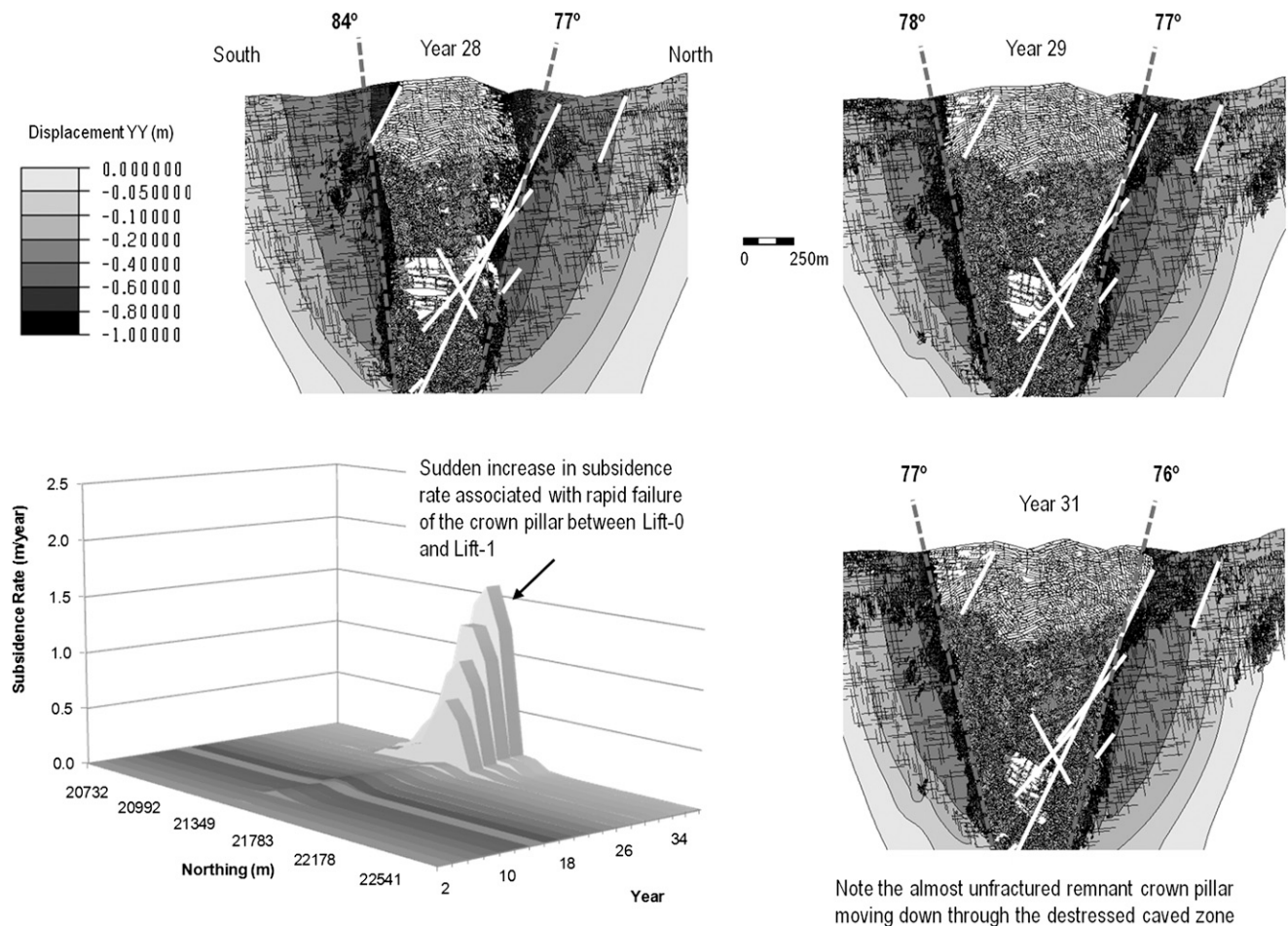


Fig. 17. Model 15100E, extent of caved zones and estimated angles of break at Years 28, 29, and 31, respectively, and subsidence rate (m/year); major geological faults are shown as lines

limitations of empirical methods and also provide an opportunity to increase our fundamental understanding of the factors governing various rock engineering problems. For instance, rock mass strength estimates developed from empirical studies may fail to predict significantly the different strength estimates associated with a different combination of fracture intensity and jointing conditions. The introduction of synthetic rock mass properties has been demonstrated to provide a better understanding of the mechanical behavior of the rock mass response in tension/shear and compression states.

Numerical and empirical techniques share the same limitations with respect to the need for an accurate representation of the structural character of the rock mass and the assumed joint properties. Ultimately, any numerical formulation applied to rock engineering problems requires a correct balance of engineering judgment, the integration of characterized field data, and numerical modeling. As shown in this paper, in their general formulation FDEM approaches are well suited to address the natural nonuniformity of geological materials and the difficulty associated with representing accurate and realistic fracture system geometry.

References

- Alzo'ubi, A. M. (2009). "The effect of tensile strength on the stability of rock slopes." Ph.D. thesis, Univ. of Alberta, Edmonton, AB, Canada.
- Barla, M., Piovano, G., and Grasselli, G. (2011). "Rock slide simulation with the combined finite discrete element method." *Int. J. Geomech.*, 12(Special Issue), 711–721.
- Barton, N., et al. (1994). "Predicted and measured performance of the 62m span Norwegian Olympic ice hockey cavern at Gjørvik." *Int. J. Rock Mech. Min. Sci. Geomech. Abstr.*, 31(6), 617–641.
- Cai, M., and Horii, H. (1993). "A constitutive model and FEM analysis of jointed rock masses." *Int. J. Rock Mech. Min. Sci. Geomech. Abstr.*, 30(4), 351–359.
- Cundall, P. A., and Damjanac, B. (2009). "A comprehensive 3D model for rock slopes based on micromechanics." *Proc., Slope Stability 2009*, Univ. de Los Andes, Santiago, Chile.
- Curran, J. H., and Ofoegbu, G. I. (1993). "Modeling discontinuities in numerical analysis." *Comprehensive Rock Engineering*, Vol. 1, J. A. Hudson, ed., Pergamon, Oxford, U.K., 443–468.
- Eberhardt, E., Stead, D., and Coggan, J. S. (2004). "Numerical analysis of initiation and progressive failure in natural rock slopes—the 1991 Randa rockslide." *Int. J. Rock Mech. Min. Sci.*, 41(1), 69–87.
- Elmo, D. (2006). "Evaluation of a hybrid FEM/DEM approach for determination of rock mass strength using a combination of discontinuity mapping and fracture mechanics modeling, with particular emphasis on modeling of jointed pillars." Ph.D. thesis, Camborne School of Mines, Univ. of Exeter, Devon, Exeter, U.K.
- Elmo, D., et al. (2007). "Integrated modeling of subsidence mechanisms and impacts due to mine caving." *Proc., 109th Canadian Institute of Mining, Metallurgy, and Petroleum (CIM) Annual General Meeting Energy & Mines Conf.*, Canadian Institute of Mining, Montreal.
- Elmo, D., Rogers, S., Beddoes, R., and Catalan, A. (2010). "An Integrated FEM/DEM-DFN synthetic rock mass approach for the modeling of

- surface subsidence associated with panel cave mining at the Cadia East Underground Project." *Proc., 2nd Int. Symp. on Block and Sublevel Caving*, Y. Potvin, ed., Australian Centre for Geomechanics, Perth, Australia.
- Elmo, D., Schlotfeldt, P., Beddoes, R., and Roberts, D. (2011). "Numerical simulations of scale effects under varying loading conditions for naturally fractured rock masses and implications for rock mass strength characterization and the design of overhanging rock slopes." *Proc., 45th U.S. Rock Mech. Symp.*, American Rock Mechanics Association, San Francisco.
- Elmo, D., and Stead, D. (2010). "An integrated numerical modeling—discrete fracture network approach applied to the characterization of rock mass strength of naturally fractured pillars." *Rock Mech. Rock Eng.*, 43(1), 3–19.
- Elmo, D., Vyazmensky, A., Stead, D., and Rance, J. (2008). "Numerical analysis of pit wall deformation induced by block-caving mining: A combined FEM/DEM-DFN synthetic rock mass approach." *Proc., 5th Conf. and Exhibition on Mass Mining*, H. Schunnesson and E. Nordlund, eds., Lulea, Sweden.
- Franz, J. (2009). "An investigation of combined failure mechanisms in large scale open pit slopes." Ph.D. thesis, School of Mining Engineering, Univ. of New South Wales, Sydney, Australia.
- Hajiabdolmajid, V., Kaiser, P. K., and Martin, C. D. (2002). "Modeling brittle failure of rock." *Int. J. Rock Mech. Min. Sci.*, 39(6), 731–741.
- Hoek, E. (2007). "Practical rock engineering." (<http://www.rocksience.com>) (Jun. 30, 2013).
- Hoek, E., and Brown, E. T. (1980). *Underground excavations in rock*, Institution of Mining and Metallurgy, London.
- Hoek, E. T., Carranza Torres, C., and Corkum, B. (2002). "Hoek-Brown failure criterion—2002 edition." *Proc., Fifth North American Rock Mech. Symp. (NARMS-TAC)*, University of Toronto Press, Toronto, 267–273.
- Hoek, E. T., Kaiser, P. K., and Bawden, W. F. (1995). *Support of underground excavations in hard rock*, A.A. Balkema, Rotterdam, Netherlands.
- Hoek, E. T., Wood, D., and Shah, S. (1992). "A modified Hoek-Brown criterion for jointed rock masses." *Proc., Rock Characterization: Int. Society for Rock Mechanics (ISRM) Symp., Eurock '92*, Thomas Telford, London, 209–214.
- Jiang, M., Leroueil, S., Zhu, H., Yu, S., and Konrad, J. M. (2009). "Two-dimensional discrete element theory for rough particles." *Int. J. Geomech.*, 9(1), 20–33.
- Jing, L. (1998). "Formulation of discontinuous deformation analysis (DDA)—an implicit discrete element model for block systems." *Eng. Geol.*, 49(3–4), 371–381.
- Karami, A., and Stead, D. (2008). "Asperity degradation and damage in the direct shear test: A hybrid DEM/FEM approach." *Rock Mech. Rock Eng.*, 41(2), 229–266.
- Klerck, P. A. (2000). "The finite element modeling of discrete fracture in quasi-brittle materials." Ph.D. thesis, Univ. of Swansea, Swansea, U.K.
- Klerck, P. A., Sellers, E. J., and Owen, D. R. J. (2004). "Discrete fracture in quasi-brittle materials under compressive and tensile stress states." *Comput. Methods Appl. Mech. Eng.*, 193(27), 3035–3056.
- Mahabadi, O. K., Lisjak, A., Munjiza, A., and Grasselli, G. (2012). "Y-Geo: A new combined finite-discrete element numerical code for geomechanical applications." *Int. J. Geomech.*, 12(Special Issue), 676–688.
- Mas Ivars, D. (2010). "Bonded particle model for jointed rock mass." Ph.D. thesis, KTH Royal Institute of Technology, Stockholm, Sweden.
- Mogi, K. (1967). "Effect of the intermediate principal stress on rock failure." *J. Geophys. Res.*, 72(20), 5117–5131.
- Munjiza, A. (2004). *The combined finite-discrete element method*, Wiley, Hoboken, NJ.
- Nordlund, E., Radberg, G., and Jing, L. (1995). "Determination of failure modes in jointed pillars by numerical modeling." *Fractured and jointed rock masses*, A. A. Balkema, Rotterdam, Netherlands, 345–350.
- Ostojca-Starzewski, M. (2002). "Lattice models in micromechanics." *Appl. Mech. Rev.*, 55(1), 35–59.
- Owen, D. R. J., et al. (2004a). "The modeling of multi-fracturing solids and particulate media." *Int. J. Numer. Methods Eng.*, 60(1), 317–339.
- Owen, D. R. J., Pires, F. M., De Souza Neto, E. A., and Feng, Y. T. (2004b). "Continuous/discrete strategies for the modeling of fracturing solids." *Publication of the Civil & Computational Eng. Centre*, Univ. of Wales, Swansea, U.K.
- Pierce, M., Cundall, P., Potyondy, D., and Mas Ivars, D. (2007). "A synthetic rock mass model for jointed rock." *Proc., 1st Canada-U.S. Rock Mech. Symp.*, Vol. 1, Taylor & Francis, London, 341–349.
- Pierce, M. P., Gaida, M., and DeGagne, D. (2009). "Estimation of rock block strength." *Proc., 3rd Canada/US (CANUS) Rock Mechanics Symposium*, M. Diederichs and G. Grasselli, eds., Canadian Rock Mechanics Association, Toronto, Paper 4360.
- Pine, R. J., Coggan, J. S., Flynn, Z. N., and Elmo, D. (2006). "The development of a new numerical modeling approach for naturally fractured rock masses." *Rock Mech. Rock Eng.*, 39(5), 395–419.
- Pine, R. J., and Harrison, J. P. (2003). "Rock mass properties for engineering design." *Quart. J. Eng. Geol. Hydrogeol.*, 36(1), 5–16.
- Pine, R. J., Owen, D. R. J., Coggan, J. S., and Rance, J. M. (2007). "A new discrete modeling approach for rock masses." *Geotechnique*, 57(9), 757–766.
- Potyondy, D. O., and Cundall, P. A. (2004). "A bonded-particle model for rock." *Int. J. Rock Mech. Min. Sci.*, 41(8), 1329–1364.
- Rockfield. (2011). *ELFEN user's manual, version 4*, Rockfield Software Ltd., Technium, Swansea, U.K. (<http://www.rockfield.co.uk/elfen.htm>).
- Singh, M., Rao, K. S., and Ramamurthy, T. (2002). "Strength and deformational behavior of a jointed rock mass." *Rock Mech. Rock Eng.*, 35(1), 45–64.
- Stead, D., Eberhardt, E., and Coggan, J. C. (2006). "Developments in the characterization of complex rock slope deformations and failure using numerical modeling techniques." *Eng. Geol.*, 83(1–3), 217–235.
- Stead, D., Elmo, D., Yan, M., and Coggan, J. (2007). "Modeling brittle fracture in rock slopes: Experience gained and lessons learned." *Proc., Int. Symp. on Rock Slope Stability in Open Pit Mining and Civil Engineering*, Australian Centre for Geomechanics, Univ. of Western Australia, Perth, Australia.
- Vyazmensky, A. (2008). "Numerical modeling of surface subsidence associated with block cave mining using a finite element/discrete element approach." Ph.D. thesis, Simon Fraser Univ., Vancouver, BC, Canada.
- Vyazmensky, A., Elmo, D., and Stead, D. (2010a). "Role of rock mass fabric and faulting in the development of block caving induced subsidence." *Rock Mech. Rock Eng.*, 43(5), 533–556.
- Vyazmensky, A., Stead, D., Elmo, D., and Moss, A. (2010b). "Numerical analysis of block caving induced instability in large open pit slopes: A finite element/discrete element approach." *Rock Mech. Rock Eng.*, 43(1), 21–39.
- Yan, M. (2008). "Numerical modeling of brittle fracture and step-path failure: From laboratory to rock slope scale." Ph.D. thesis, Simon Fraser Univ., Vancouver, BC, Canada.
- Yumlu, M., and Ozbay, M. U. (1995). "A study of the behavior of brittle rocks under plane strain and triaxial loading conditions." *Int. J. Rock Mech. Min. Sci. Geomech. Abstr.*, 32(7), 725–733.